COMPDYN 2013
4th ECCOMAS Thematic Conference on
Computational Methods in Structural Dynamics and Earthquake Engineering
M. Papadrakakis, V. Papadopoulos, V. Plevris (eds.)
Kos Island, Greece, 12–14 June 2013

A NEW COROTATIONAL ELEMENT FOR NONLINEAR DYNAMIC ANALYSIS OF 3D BEAMS

Thanh-Nam Le [12], Jean-Marc Battini[2], and Mohammed Hjiaj[1]

[1]Université Européenne de Bretagne, INSA de Rennes - LGCGM/Structural Engineering Research Group
20 avenue des Buttes de Coësmes, CS 70839, 35708 Rennes Cedex 7, France
e-mail: Thanh-Nam.Le@insa-rennes.fr, mohammed.hjiaj@insa-rennes.fr

[2] KTH, Royal Institute of Technology - Department of Civil and Architectural Engineering, Division of Structural Engineering and Bridges
Brinellvägen 23, SE-10044 Stockholm, Sweden
e-mail: jean-marc.battini@byv.kth.se

Keywords: Corotational method, Nonlinear dynamics, 3D beam elements, Finite rotations.

Abstract. *The purpose of the paper is to present a corotational beam element for the nonlinear dynamic analysis of 3D flexible frames. The novelty of the formulation lies in the use of the corotational framework (i.e. the decomposition into rigid body motion and pure deformation) to derive not only the internal force vector and the tangent stiffness matrix but also the inertia force vector and the tangent dynamic matrix. As a consequence, cubic interpolations are adopted to formulate both inertia and internal local terms. In the derivation of the dynamic terms, an approximation for the local rotations is introduced and a concise expression for the global inertia force vector is obtained. To enhance the efficiency of the iterative procedure, an approximate expression of the tangent dynamic matrix is adopted. Several numerical examples are considered to assess the performance of the new formulation against the one suggested by Simo and Vu-Quoc [37]. It was observed that the proposed formulation proves to combine accuracy with efficiency. In particular, the present approach achieves the same level of accuracy as the formulation of Simo and Vu-Quoc but with a significantly smaller number of elements.*

1 Introduction

Flexible beams are used in many applications, for instance large deployable space structures, aircrafts and wind turbines propellers, offshore platforms. These structures undergo large displacements and finite rotations, but the strains remain small. Their nonlinear dynamic behavior is often simulated using geometrically nonlinear spatial beam elements. In the literature, several approaches have been used to develop such elements. A large number of them have been formulated in the total Lagrangian context [8, 9, 16, 20, 21, 23, 24, 28, 37, 42, 43, 44]. An other attractive way to develop effective nonlinear dynamic beam elements, which is adopted in the present work, is to use the corotational approach. Indeed, this framework has been adopted by several authors to develop efficient beam and shell elements for the nonlinear static and dynamic analysis of flexible structures. [1, 5, 7, 10, 11, 12, 14, 15, 18, 19, 22, 29, 31, 33, 38]. The main idea of the method is to decompose the motion of the element into rigid body and pure deformational parts. During the rigid body motion, a local coordinates system, attached to the element, moves and rotates with it. The deformational part is measured in this local system. The main interest of the approach is that different assumptions can be made to represent the local deformations, giving rise to different possibilities for the local element formulation.

For the geometrically and materially static nonlinear analysis of beam structures with corotational approach, several local formulations have been proposed by Battini and Pacoste [4], and Alsafadie et al. [2]. The results of a comparative study of 3D beam formulations, which can be found in [2], have shown that local beam elements based on cubic interpolations are more efficient and accurate than the ones which employ linear interpolations. However, in dynamics, one has to deal with the inertia terms which by nature are complicate to formulate. This is particularly true in the corotational formulation of Bernoulli-type beam elements. This difficulty has hampered the development of the corotational approach in nonlinear dynamics. To avoid the consistent derivation of the inertia terms, several routes have been considered.

For 2D dynamic analysis, quite a few authors [29, 31, 38] have adopted the constant lumped mass matrix without any attempt to check its accuracy. Iura and Atluri [22] suggested to simply switch to a Timoshenko beam model where the mass matrix is constant and therefore the inertial terms are simple to evaluate. Behdinan et al. [7] proposed a 2D corotational dynamic formulation where cubic interpolations have been used to describe the global displacements, which is not consistent with the idea of the corotational method as originally introduced by Nour-Omid and Rankin [30]. More recently, Le et al. [26] developed a consistent 2D corotational beam element for nonlinear dynamics. Cubic interpolations were used to describe the local displacements and to derive both inertia and internal terms. Numerical results demonstrated that the formulation is more efficient than the classic formulations (i.e. with the constant Timoshenko and the constant lumped mass matrices). For 3D dynamic analysis, Crisfield et al. [12] suggested to use a constant Timoshenko mass matrix along with local cubic interpolations to derive the internal force vector and the corresponding tangent stiffness matrix. As pointed out by Crisfield et al. [12], this combination is not consistent but it provides reasonable results when the number of elements is large enough. Hsiao et al. [19] presented a corotational formulation for the nonlinear analysis of 3D beams. However the corotational framework adopted in [19] is different from the classic one as proposed first by Nour-Omid and Rankin [30] and adopted in this paper.

The objective of this paper is to extend the consistent 2D corotational dynamic formulation presented in [26] to 3D beam structures. Hence, the corotational framework (i.e. the decomposition into rigid body motion and pure deformation) is used to derive not only the internal force vector and the tangent stiffness matrix but also the inertia force vector and the tangent dynamic matrix. The element has two nodes and is initially straight. The same cubic interpolations are adopted to formulate both inertia and internal local terms. In doing so, the complex expressions of the inertia terms are significantly simplified by adopting a proper approximation for the local rotations. To enhance the efficiency of the iterative procedure, the less significant term in the tangent dynamic matrix is ignored (see [27]).

Regarding the time-stepping scheme, the HHT α method (with $\alpha = -0.05$) is adopted in this work. This energy-dissipative method, which is implemented in several commercial FEM programs (Abaqus, Lusas) and was employed by many authors [9, 12, 24], limits the influence of high frequencies by introducing a numerical damping. The latter often avoids numerical instability, but also results in dissipation of the total energy.

Several numerical applications are presented with the objective to compare the performances of the new formulation against two other approaches. The first approach is similar to the one presented above, but linear local interpolations, instead of cubic ones, are used to derive only the dynamic terms. The purpose is to evaluate the influence of the choice of the local interpolations on the dynamic terms. The second approach is the classic total Lagrangian formulation proposed by Simo and Vu-Quoc [35, 36, 37].

The paper is organized as follows. Section 2 presents some aspects of the parametrization of finite rotations that are essentials for the subsequent developments. Section 3 is devoted to the corotational beam kinematics, whilst the local beam element formulation is introduced in Section 4. The internal force vector and the tangent stiffness matrix are briefly presented in Section 5. More details about the derivation can be found in [4]. Sections 6 focus on the derivation of the inertia terms. In Section 7, several examples are presented in order to assess the accuracy of the present dynamic formulation. Finally, conclusions are given in Section 8.

2 Parametrization of finite rotations

In this section, the relations required for the development of the present formulation are introduced. For a more complete description about the finite rotations, the reader is referred to textbooks and papers such as [3, 6, 13, 17, 25, 39, 40].

The coordinate of a vector $\mathbf{x}_o$ that is rotated into the position $\mathbf{x}$ (see Fig. 1) is given by the relation

$$\mathbf{x} = \mathbf{R}\,\mathbf{x}_o \,. \tag{1}$$

Due to its orthonormality, the rotation matrix $\mathbf{R}$ can be parameterized using only three independent parameters. One possibility is to use the rotational vector defined by

$$\boldsymbol{\theta} = \theta\,\mathbf{n}\,, \tag{2}$$

where $\mathbf{n}$ is a unit vector defining the axis of the rotation and $\theta = (\boldsymbol{\theta}^{\mathrm{T}}\boldsymbol{\theta})^{1/2}$ is the angle of the

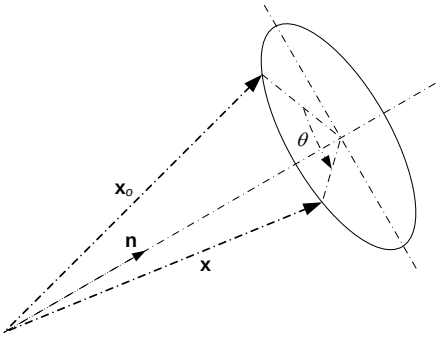

Figure 1: Finite rotation of a vector.

rotation.

The relation between the rotation matrix and the rotational vector is given by the Rodrigues' formula

$$\mathbf{R} = \mathbf{I} + \frac{\sin\theta}{\theta}\widetilde{\boldsymbol{\theta}} + \frac{1-\cos\theta}{\theta^2}\widetilde{\boldsymbol{\theta}}\widetilde{\boldsymbol{\theta}} = \exp(\widetilde{\boldsymbol{\theta}})\,, \tag{3}$$

where $\widetilde{\boldsymbol{\theta}}$ is the skew matrix associated with the vector $\boldsymbol{\theta}$, $\mathbf{I}$ is the 3×3 identity matrix.
The variation $\delta\mathbf{R}$ of the rotation matrix $\mathbf{R}$ is calculated according to

$$\delta\mathbf{R} = \widetilde{\delta\mathbf{w}}\mathbf{R}\,. \tag{4}$$

$\delta\mathbf{w}$, which is also denoted as spatial spin variables, is related to the variation of the rotational vector through

$$\delta\mathbf{w} = \mathbf{T}_s(\boldsymbol{\theta})\,\delta\boldsymbol{\theta}\,, \tag{5}$$

with

$$\mathbf{T}_s(\boldsymbol{\theta}) = \mathbf{I} + \frac{1-\cos\theta}{\theta^2}\widetilde{\boldsymbol{\theta}} + \frac{\theta-\sin\theta}{\theta^3}\widetilde{\boldsymbol{\theta}}\widetilde{\boldsymbol{\theta}}\,. \tag{6}$$

3 Beam kinematics

In this work, the corotational framework introduced by Nour-Omid and Rankin [30], and further developed by Pacoste and Eriksson [32] and Battini and Pacoste [4] is fully adopted.

The definition of the corotational two node beam element described in this section involves several coordinate systems, see Fig. 2. First a global reference system is defined by the triad of unit orthogonal vectors $\mathbf{e}_\alpha$ $(\alpha = 1,2,3)$. Next, a local system which continuously rotates and translates with the element is selected. The orthonormal basis vectors of the local system are denoted by $\mathbf{r}_\alpha$ $(\alpha = 1,2,3)$. In the initial (undeformed) configuration, the local system is defined by the orthonormal triad $\mathbf{e}^o_\alpha$. In addition, $\mathbf{t}^1_\alpha$ and $\mathbf{t}^2_\alpha$ $(\alpha = 1,2,3)$, denote two unit triads rigidly attached to nodes 1 and 2. The origin of the local system is taken at node 1 and thus the rigid translation is defined by $\mathbf{u}^g_1$, the translation at node 1. Here and in the sequel, superscript g

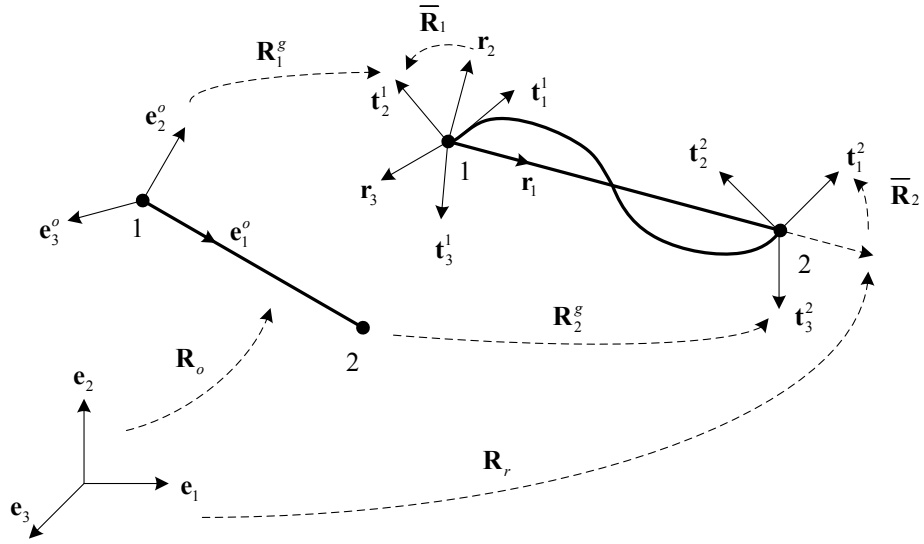

Figure 2: Beam kinematics and the coordinate systems.

indicates quantities expressed in the global reference system. The rigid rotation is such that the new orientation of the local reference system is defined by an orthogonal matrix $\mathbf{R}_r$, given by

$$\mathbf{R}_r = [\,\mathbf{r}_1\ \mathbf{r}_2\ \mathbf{r}_3\,]\,. \tag{7}$$

The first coordinate axis of the local system is defined by the line connecting nodes 1 and 2 of the element. Consequently, $\mathbf{r}_1$ is given by

$$\mathbf{r}_1 = \frac{\mathbf{x}_2^g + \mathbf{u}_2^g - \mathbf{x}_1^g - \mathbf{u}_1^g}{l_n}\,, \tag{8}$$

with $\mathbf{x}_i^g$ $(i = 1,2)$ denoting the nodal coordinates in the initial undeformed configuration and l_n denoting the current length of the beam, i.e.

$$l_n = \|\mathbf{x}_2^g + \mathbf{u}_2^g - \mathbf{x}_1^g - \mathbf{u}_1^g\|\,. \tag{9}$$

The remaining two axes are determined with the help of an auxiliary vector $\mathbf{p}$. In the initial configuration $\mathbf{p}$ is directed along the local $\mathbf{e}_2^o$ direction, whereas in the deformed configuration its orientation is obtained from

$$\mathbf{p} = \frac{1}{2}(\mathbf{p}_1 + \mathbf{p}_2)\,, \qquad \mathbf{p}_i = \mathbf{R}_i^g\,\mathbf{R}_o\,[0\ 1\ 0]^{\mathrm{T}} \qquad (i = 1,2)\,, \tag{10}$$

where $\mathbf{R}_1^g$ and $\mathbf{R}_2^g$ are the orthogonal matrices used to specify the orientation of the nodal triads $\mathbf{t}_\alpha^1$ and $\mathbf{t}_\alpha^2$ respectively, and $\mathbf{R}_o$ specifies the orientation of the local frame in the initial configuration, i.e. $\mathbf{R}_o = [\mathbf{e}_1^o\ \mathbf{e}_2^o\ \mathbf{e}_3^o]$. The unit vectors $\mathbf{r}_2$ and $\mathbf{r}_3$ are then computed by the following vector products

$$\mathbf{r}_3 = \frac{\mathbf{r}_1 \times \mathbf{p}}{\|\mathbf{r}_1 \times \mathbf{p}\|}, \qquad \mathbf{r}_2 = \mathbf{r}_3 \times \mathbf{r}_1\,, \tag{11}$$

resulting in the orthogonal matrix $\mathbf{R}_r$ (Eq. (7)) being completely determined.

The rigid motion previously described, is accompanied by local deformational displacements and rotations with respect to the local element axes. In this context, due to the particular choice of the local system, the local translations at node 1 are zero. Moreover, at node 2, the only non zero component is the translation along $\mathbf{r}_1$. This can easily be evaluated according to

$$\overline{u} = l_n - l_o\,, \tag{12}$$

with l_o denoting the length of the beam in the original undeformed configuration. Here and in the sequel, an overbar denotes a deformational kinematic quantity.

The global rotations at node i can be expressed in terms of the rigid rotation of the local axes, defined by $\mathbf{R}_r$, followed by a local rotation relative to these axes. The latter is defined by the orthogonal matrix $\overline{\mathbf{R}}_i$. Consequently, the orientation of the nodal triad $\mathbf{t}^i_\alpha$ can be obtained by means of the product $\mathbf{R}_r\,\overline{\mathbf{R}}_i$. On the other hand, (see Fig. 2) this orientation can also be obtained through the product $\mathbf{R}^g_i\,\mathbf{R}_o$, which gives

$$\overline{\mathbf{R}}_i = \mathbf{R}_r^{\mathrm{T}}\,\mathbf{R}^g_i\,\mathbf{R}_o \qquad (i=1,2)\,. \tag{13}$$

The local rotations are then evaluated from

$$\overline{\boldsymbol{\theta}}_i = \log\left(\overline{\mathbf{R}}_i\right) \qquad (i=1,2)\,. \tag{14}$$

Due to the choice of the local coordinate system, the local nodal displacement vector $\mathbf{d}_l$ has only seven components and is given by

$$\mathbf{d}_l = \left[\,\overline{u}\;\;\overline{\boldsymbol{\theta}}_1^{\mathrm{T}}\;\;\overline{\boldsymbol{\theta}}_2^{\mathrm{T}}\,\right]^{\mathrm{T}}. \tag{15}$$

The variation of the local nodal displacement vector is

$$\delta\mathbf{d}_l = \left[\,\delta\overline{u}\;\;\delta\overline{\boldsymbol{\theta}}_1^{\mathrm{T}}\;\;\delta\overline{\boldsymbol{\theta}}_2^{\mathrm{T}}\,\right]^{\mathrm{T}}, \tag{16}$$

and the global counterpart is given by

$$\delta\mathbf{d}_g = \left[\,\delta\mathbf{u}_1^{g\mathrm{T}}\;\;\delta\mathbf{w}_1^{g\mathrm{T}}\;\;\delta\mathbf{u}_2^{g\mathrm{T}}\;\;\delta\mathbf{w}_2^{g\mathrm{T}}\,\right]^{\mathrm{T}}, \tag{17}$$

with $\delta\mathbf{w}^g_i\;(i=1,2)$ denoting spatial spin variables defined by

$$\delta\mathbf{R}^g_i = \widetilde{\delta\mathbf{w}^g_i}\,\mathbf{R}^g_i\,. \tag{18}$$

For the rotational terms, the variation of Eq. (13) is needed

$$\delta\overline{\mathbf{R}}_i = \delta\mathbf{R}_r^{\mathrm{T}}\,\mathbf{R}^g_i\,\mathbf{R}_o + \mathbf{R}_r^{\mathrm{T}}\,\delta\mathbf{R}^g_i\,\mathbf{R}_o\,, \tag{19}$$

where $\delta\overline{\mathbf{R}}_i$ and $\delta\mathbf{R}_r$ are computed using Eq. (4), i.e.

$$\delta\overline{\mathbf{R}}_i = \widetilde{\delta\overline{\mathbf{w}}_i}\,\overline{\mathbf{R}}_i, \qquad \delta\mathbf{R}_r = \widetilde{\delta\mathbf{w}^g_r}\,\mathbf{R}_r\,. \tag{20}$$

$\delta\mathbf{R}_r^{\mathrm{T}}$ is calculated via the orthogonality condition $\mathbf{R}_r\,\mathbf{R}_r^{\mathrm{T}} = \mathbf{I}$. Taking variation of this relation and combining the outcome with Eq. (20) results in

$$\delta\mathbf{R}_r^{\mathrm{T}} = -\mathbf{R}_r^{\mathrm{T}}\,\widetilde{\delta\mathbf{w}^g_r}\,. \tag{21}$$

Using Eqs. (18), (20) and (21), Eq. (19) can be rewritten as

$$\widetilde{\delta\overline{\mathbf{w}}_i}\,\overline{\mathbf{R}}_i \;=\; (\widetilde{\delta\mathbf{w}_i^e} - \widetilde{\delta\mathbf{w}_r^e})\,\overline{\mathbf{R}}_i\,, \tag{22}$$

where use of Eq. (13) has been made along the fact that $\mathbf{R}_r$ transforms a vector and a tensor from global to local coordinates according to

$$\mathbf{x}^e = \mathbf{R}_r^{\mathrm{T}}\,\mathbf{x}^g, \qquad \widetilde{\mathbf{x}^e} = \mathbf{R}_r^{\mathrm{T}}\,\widetilde{\mathbf{x}^g}\,\mathbf{R}_r\,. \tag{23}$$

Thus, Eq. (22) gives

$$\delta\overline{\mathbf{w}}_i = \delta\mathbf{w}_i^e - \delta\mathbf{w}_r^e \qquad (i=1,2)\,. \tag{24}$$

Further, let

$$\delta\mathbf{d}_g^e = \mathbf{E}^{\mathrm{T}}\,\delta\mathbf{d}_g, \qquad \mathbf{E} = \begin{bmatrix} \mathbf{R}_r & \mathbf{0} & \mathbf{0} & \mathbf{0} \\ \mathbf{0} & \mathbf{R}_r & \mathbf{0} & \mathbf{0} \\ \mathbf{0} & \mathbf{0} & \mathbf{R}_r & \mathbf{0} \\ \mathbf{0} & \mathbf{0} & \mathbf{0} & \mathbf{R}_r \end{bmatrix}, \tag{25}$$

with $\mathbf{0}$ denoting the 3×3 zero matrix.
Eq. (24) can be rewritten as

$$\begin{bmatrix} \delta\overline{\mathbf{w}}_1 \\ \delta\overline{\mathbf{w}}_2 \end{bmatrix} = \left(\begin{bmatrix} \mathbf{0} & \mathbf{I} & \mathbf{0} & \mathbf{0} \\ \mathbf{0} & \mathbf{0} & \mathbf{0} & \mathbf{I} \end{bmatrix} - \begin{bmatrix} \mathbf{G}^{\mathrm{T}} \\ \mathbf{G}^{\mathrm{T}} \end{bmatrix} \right) \mathbf{E}^{\mathrm{T}}\,\delta\mathbf{d}_g = \mathbf{P}\mathbf{E}^{\mathrm{T}}\,\delta\mathbf{d}_g\,, \tag{26}$$

where the matrix $\mathbf{G}$ is defined by

$$\mathbf{G}^{\mathrm{T}} = \frac{\partial\mathbf{w}_r^e}{\partial\mathbf{d}_g^e}\,. \tag{27}$$

The expression of $\mathbf{G}$ is given by

$$\mathbf{G}^{\mathrm{T}} = \begin{bmatrix} 0 & 0 & \dfrac{\eta}{l_n} & \dfrac{\eta_{12}}{2} & -\dfrac{\eta_{11}}{2} & 0 & 0 & 0 & -\dfrac{\eta}{l_n} & \dfrac{\eta_{22}}{2} & -\dfrac{\eta_{21}}{2} & 0 \\ 0 & 0 & \dfrac{1}{l_n} & 0 & 0 & 0 & 0 & 0 & -\dfrac{1}{l_n} & 0 & 0 & 0 \\ 0 & -\dfrac{1}{l_n} & 0 & 0 & 0 & 0 & 0 & \dfrac{1}{l_n} & 0 & 0 & 0 & 0 \end{bmatrix}, \tag{28}$$

$$\eta = \frac{p_1}{p_2} \qquad \eta_{11} = \frac{p_{11}}{p_2}\,, \qquad \eta_{12} = \frac{p_{12}}{p_2} \qquad \eta_{21} = \frac{p_{21}}{p_2} \qquad \eta_{22} = \frac{p_{22}}{p_2}\,, \tag{29}$$

where (see Eq. (10)) p_j and p_{ij} are the components of the vectors $\mathbf{R}_r^{\mathrm{T}}\,\mathbf{p}$ and $\mathbf{R}_r^{\mathrm{T}}\,\mathbf{p}_i$, respectively.

4 Local beam kinematic description

In this section, the local beam kinematics, adopted to derive both inertia and internal terms, is presented. The local motion of a beam cross-section from the initial (i.e. rotated but still undeformed) configuration to the current configuration is defined by the translation of the cross-section centroid G and the rotation of the section (see Figs. 3 and 4).

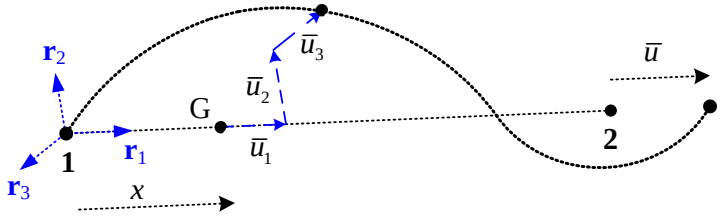

Figure 3: Local beam configuration - Translation.

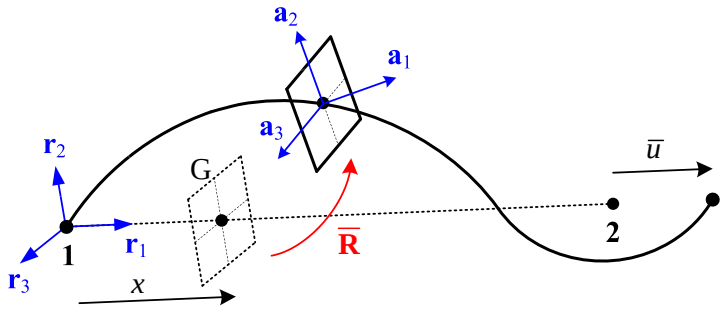

Figure 4: Local beam configuration - Rotation.

Let $[\bar{u}_1 \;\; \bar{u}_2 \;\; \bar{u}_3]^{\mathrm{T}}$ and $\bar{\boldsymbol{\theta}} = [\bar{\theta}_1 \;\; \bar{\theta}_2 \;\; \bar{\theta}_3]^{\mathrm{T}}$ denote the local displacement vector of G and the local rotation of the section, respectively. These quantities are interpolated from the local nodal values based on the Bernoulli hypothesis. Then, due to the particular choice of the local degrees of freedom, one has

$$\begin{bmatrix} \bar{u}_1 \\ \bar{u}_2 \\ \bar{u}_3 \\ \bar{\theta}_1 \\ \bar{\theta}_2 \\ \bar{\theta}_3 \end{bmatrix} = \begin{bmatrix} N_2 & 0 & 0 & 0 & 0 & 0 & 0 \\ 0 & 0 & 0 & N_3 & 0 & 0 & N_4 \\ 0 & 0 & -N_3 & 0 & 0 & -N_4 & 0 \\ 0 & N_1 & 0 & 0 & N_2 & 0 & 0 \\ 0 & 0 & N_5 & 0 & 0 & N_6 & 0 \\ 0 & 0 & 0 & N_5 & 0 & 0 & N_6 \end{bmatrix} \mathbf{d}_l \,, \tag{30}$$

where the local nodal displacement vector $\mathbf{d}_l$ is defined by Eq. (15).
The expressions of the interpolation functions are given by

$$N_1 = 1 - \frac{x}{l_o}, \qquad N_2 = \frac{x}{l_o}, \qquad N_3 = x\left(1 - \frac{x}{l_o}\right)^2,$$
$$N_4 = -\left(1 - \frac{x}{l_o}\right)\frac{x^2}{l_o}, \quad N_5 = \left(1 - \frac{3x}{l_o}\right)\left(1 - \frac{x}{l_o}\right), \quad N_6 = \left(\frac{3x}{l_o} - 2\right)\frac{x}{l_o}.$$

Let $\mathbf{u}_l = [0 \;\; \bar{u}_2 \;\; \bar{u}_3]^{\mathrm{T}}$ denotes the local transverse displacement vector. This vector is calculated by

$$\mathbf{u}_l = \mathbf{P}_1 \begin{bmatrix} \bar{\boldsymbol{\theta}}_1 \\ \bar{\boldsymbol{\theta}}_2 \end{bmatrix}, \quad \mathbf{P}_1 = \begin{bmatrix} 0 & 0 & 0 & 0 & 0 & 0 \\ 0 & 0 & N_3 & 0 & 0 & N_4 \\ 0 & -N_3 & 0 & 0 & -N_4 & 0 \end{bmatrix}. \tag{31}$$

The local rotation of the cross-section is evaluated as follows

$$\overline{\boldsymbol{\theta}} = \mathbf{P}_2 \begin{bmatrix} \overline{\boldsymbol{\theta}}_1 \\ \overline{\boldsymbol{\theta}}_2 \end{bmatrix}, \quad \mathbf{P}_2 = \begin{bmatrix} N_1 & 0 & 0 & N_2 & 0 & 0 \\ 0 & N_5 & 0 & 0 & N_6 & 0 \\ 0 & 0 & N_5 & 0 & 0 & N_6 \end{bmatrix}. \tag{32}$$

In the present formulation, bending shear deformations are not considered. Such deformations can easily be introduced by modifying the Hermitian shape functions as suggested in the Interdependent Interpolation Element (IIE) formulation [34].

5 Internal force vector and tangent stiffness matrix

The purpose of this section is to present briefly the derivation of the inertial force vector and the tangent stiffness matrix. A complete description can be found in [4].
Using the local beam kinematics presented in Section 4 together with a shallow arch strain description, the local internal force vector $\mathbf{f}_l$ and the local tangent stiffness matrix $\mathbf{K}_l$ associated with $\delta\mathbf{d}_l$ (see Eq. (16)) are computed. The Maple codes for $\mathbf{f}_l$ and $\mathbf{K}_l$ are given in [4].
The global internal force vector $\mathbf{f}_{\mathrm{g}}$ and the global tangent stiffness matrix $\mathbf{K}_{\mathrm{g}}$ associated with $\delta\mathbf{d}_g$ (see Eq. (17)) are obtained through a change of variables based on the transformation matrix $\mathbf{B}$ defined by

$$\delta\mathbf{d}_l = \mathbf{B}\,\delta\mathbf{d}_g\,. \tag{33}$$

By equating the internal virtual work in both the global and local systems, the expression of the global internal force vector $\mathbf{f}_{\mathrm{g}}$ is obtained as

$$\mathbf{f}_{\mathrm{g}} = \mathbf{B}^{\mathrm{T}}\mathbf{f}_l\,. \tag{34}$$

By taking the variations of Eq. (34), the expression of the global tangent stiffness matrix $\mathbf{K}_{\mathrm{g}}$ is obtained

$$\mathbf{K}_{\mathrm{g}} = \mathbf{B}^{\mathrm{T}}\mathbf{K}_l\mathbf{B} + \left.\frac{\partial(\mathbf{B}^{\mathrm{T}}\mathbf{f}_l)}{\partial\mathbf{d}_g}\right|_{\mathbf{f}_l}. \tag{35}$$

The details regarding the final expressions of $\mathbf{f}_{\mathrm{g}}$ and $\mathbf{K}_{\mathrm{g}}$ are given in [4].

6 Inertia force vector and tangent dynamic matrix

This section is devoted to the derivation of the inertia force vector and the tangent dynamic matrix. The novelty of the approach presented here is that the same corotational kinematics description is adopted to formulate both inertia and internal terms, which ensures the consistency of the formulation. As already mentioned, the current 3D formulation is the extension of the 2D one proposed by the authors [26].

Using the cross-section centroid as the reference point, the variation of the kinetic energy can be expressed as (see [17])

$$\delta K = -\int_{l_o} \left\{ \delta\mathbf{u}^{\mathrm{T}} A_\rho \ddot{\mathbf{u}} + \delta\mathbf{w}^{\mathrm{T}} \left[\mathbf{I}_\rho \dot{\mathbf{w}} + \widetilde{\dot{\mathbf{w}}}\mathbf{I}_\rho \mathbf{w} \right] \right\} \mathrm{d}l\,, \tag{36}$$

where $\dot{\mathbf{u}}$, $\dot{\mathbf{w}}$ are the translational and angular velocity of the cross-section. Please note that in order to simplify the notations, in this section, the superscripts "g" which refer to global

quantities are dropped for $\mathbf{u}$, $\dot{\mathbf{w}}$ and their derivatives.
$\mathbf{I}_\rho$ is the spatial inertia dyadic tensor given by

$$\mathbf{I}_\rho = \mathbf{R}^g \mathbf{R}_o \mathbf{J}_\rho \left(\mathbf{R}^g \mathbf{R}_o\right)^{\mathrm{T}}, \tag{37}$$

in which $\mathbf{J}_\rho$ is the inertia dyadic of the cross-section in the initial configuration.
The inertia force vector is then derived from the following relation

$$\delta K = -\mathbf{f}_{\mathrm{k}}^{\mathrm{T}} \delta \mathbf{d}_g \,. \tag{38}$$

6.1 Translational displacement variables

The position of the cross-section centroid in the global coordinate system is given by (see Fig. 3)

$$\mathrm{OG} = \mathbf{x}_1^g + \mathbf{u}_1^g + (x + \overline{u}_1)\,\mathbf{r}_1 + \overline{u}_2 \mathbf{r}_2 + \overline{u}_3 \mathbf{r}_3 \,. \tag{39}$$

By using Eqs. (8), (12) and (30), one obtains

$$\mathrm{OG} = N_1 \mathbf{x}_1^g + N_2 \mathbf{x}_2^g + N_1 \mathbf{u}_1^g + N_2 \mathbf{u}_2^g + \mathbf{R}_r \mathbf{u}_l \,. \tag{40}$$

Then by taking the variation of the above equation, the following expression is obtained

$$\delta \mathrm{OG} = \delta \mathbf{u} = \mathbf{N}\, \delta \mathbf{d}_g + \mathbf{R}_r \delta \mathbf{u}_l + \delta \mathbf{R}_r \mathbf{u}_l \,, \tag{41}$$

with $\mathbf{N} = \begin{bmatrix} N_1\mathbf{I} & \mathbf{0} & N_2\mathbf{I} & \mathbf{0} \end{bmatrix}$.
One interesting property of $\mathbf{N}$ is that

$$\mathbf{N} = \mathbf{R}_r \mathbf{N} \mathbf{E}^{\mathrm{T}} . \tag{42}$$

The variation $\delta \mathbf{R}_r$ is calculated using Eqs. (20) and (23) as

$$\delta \mathbf{R}_r = \mathbf{R}_r \widetilde{\delta \mathbf{w}_r^e} . \tag{43}$$

From Eqs. (25) and (27), $\delta \mathbf{w}_r^e$ is obtained as

$$\delta \mathbf{w}_r^e = \mathbf{G}^{\mathrm{T}} \mathbf{E}^{\mathrm{T}}\, \delta \mathbf{d}_g \,. \tag{44}$$

By taking the differentiation of Eq. (31), one obtains

$$\delta \mathbf{u}_l = \mathbf{P}_1 \begin{bmatrix} \delta \overline{\boldsymbol{\theta}}_1 \\ \delta \overline{\boldsymbol{\theta}}_2 \end{bmatrix} . \tag{45}$$

In the corotational approach, the local rotations at the nodes $\overline{\boldsymbol{\theta}}_i$ $(i = 1,2)$, defined in Eq. (14), are small and the operator $\mathbf{T}_s(\overline{\boldsymbol{\theta}}_i)$ is close to the identity matrix. Consequently, see Eq. (5), the following approximation is adopted

$$\delta \overline{\mathbf{w}}_i \approx \delta \overline{\boldsymbol{\theta}}_i \,. \tag{46}$$

Then, using Eqs. (26) and (46), the expression in (45) becomes

$$\delta \mathbf{u}_l \approx \mathbf{P}_1 \begin{bmatrix} \delta \overline{\mathbf{w}}_1 \\ \delta \overline{\mathbf{w}}_2 \end{bmatrix} = \mathbf{P}_1 \mathbf{P} \mathbf{E}^{\mathrm{T}}\, \delta \mathbf{d}_g \,. \tag{47}$$

Inserting Eqs. (42) - (44) and (47) into Eq. (41), one obtains

$$\delta\mathbf{u} = \mathbf{R}_r \mathbf{H}_1 \mathbf{E}^{\mathrm{T}} \delta\mathbf{d}_g \,, \tag{48}$$

with

$$\mathbf{H}_1 = \mathbf{N} + \mathbf{P}_1 \mathbf{P} - \widetilde{\mathbf{u}}_l \mathbf{G}^{\mathrm{T}} \,. \tag{49}$$

Obviously, the translational velocity of the cross-section centroid is evaluated from

$$\dot{\mathbf{u}} = \mathbf{R}_r \mathbf{H}_1 \mathbf{E}^{\mathrm{T}} \dot{\mathbf{d}}_g \,. \tag{50}$$

By taking the time derivative of the above equation, the expression of the translational acceleration reads as follows

$$\ddot{\mathbf{u}} = \mathbf{R}_r \mathbf{H}_1 \mathbf{E}^{\mathrm{T}} \ddot{\mathbf{d}}_g + \mathbf{R}_r \mathbf{C}_1 \mathbf{E}^{\mathrm{T}} \dot{\mathbf{d}}_g = \mathbf{R}_r \ddot{\mathbf{u}}^e \,, \tag{51}$$

with

$$\mathbf{C}_1 = \widetilde{\dot{\mathbf{w}}_r^e} \mathbf{H}_1 + \dot{\mathbf{H}}_1 - \mathbf{H}_1 \mathbf{E}_t \,, \qquad \mathbf{E}_t = \begin{bmatrix} \widetilde{\dot{\mathbf{w}}_r^e} & \mathbf{0} & \mathbf{0} & \mathbf{0} \\ \mathbf{0} & \widetilde{\dot{\mathbf{w}}_r^e} & \mathbf{0} & \mathbf{0} \\ \mathbf{0} & \mathbf{0} & \widetilde{\dot{\mathbf{w}}_r^e} & \mathbf{0} \\ \mathbf{0} & \mathbf{0} & \mathbf{0} & \widetilde{\dot{\mathbf{w}}_r^e} \end{bmatrix} , \tag{52}$$

and $\dot{\mathbf{H}}_1$ given in Appendix A.

6.2 Finite rotation variables

Using Eqs. (23) and (24), the spatial spin variables, associated to the global rotation of a cross-section, are evaluated using

$$\delta\mathbf{w} = \mathbf{R}_r \delta\mathbf{w}^e = \mathbf{R}_r \left(\delta\mathbf{w}_r^e + \delta\overline{\mathbf{w}} \right) . \tag{53}$$

Combining Eq. (32) with the approximation defined in Eq. (46) and using Eq. (26), the local spatial spin variables are calculated as follows

$$\delta\overline{\mathbf{w}} = \mathbf{P}_2 \mathbf{P} \mathbf{E}^{\mathrm{T}} \delta\mathbf{d}_g \,. \tag{54}$$

Finally, by introducing Eqs. (44) and (54) into (53), the spatial spin variables are computed from the global nodal displacement vector by

$$\delta\mathbf{w} = \mathbf{R}_r \mathbf{H}_2 \mathbf{E}^{\mathrm{T}} \delta\mathbf{d}_g \,, \tag{55}$$

with

$$\mathbf{H}_2 = \mathbf{P}_2 \mathbf{P} + \mathbf{G}^{\mathrm{T}} \,. \tag{56}$$

The angular velocity is calculated with the following similar expression

$$\dot{\mathbf{w}} = \mathbf{R}_r \mathbf{H}_2 \mathbf{E}^{\mathrm{T}} \dot{\mathbf{d}}_g = \mathbf{R}_r \dot{\mathbf{w}}^e \,. \tag{57}$$

The angular acceleration is obtained by taking the time derivative of the angular velocity

$$\ddot{\mathbf{w}} = \mathbf{R}_r \mathbf{H}_2 \mathbf{E}^{\mathrm{T}} \ddot{\mathbf{d}}_g + \mathbf{R}_r \mathbf{C}_2 \mathbf{E}^{\mathrm{T}} \dot{\mathbf{d}}_g = \mathbf{R}_r \ddot{\mathbf{w}}^e \,, \tag{58}$$

with $\dot{\mathbf{H}}_2$ given in Appendix A and

$$\mathbf{C}_2 = \widetilde{\dot{\mathbf{w}}_r^e} \mathbf{H}_2 + \dot{\mathbf{H}}_2 - \mathbf{H}_2 \mathbf{E}_t \,. \tag{59}$$

6.3 Inertia force vector and tangent dynamic matrix

By inserting the expressions of $\delta\mathbf{u}$ and $\delta\mathbf{w}$ given in Eqs. (48) and (55) into Eq. (36), and using the local forms $\ddot{\mathbf{u}}^e$, $\dot{\mathbf{w}}^e$ and $\ddot{\mathbf{w}}^e$ (see Eqs. (51), (57) and (58)), the inertia force vector is obtained as

$$\mathbf{f}_{\mathrm{k}} = \mathbf{E}\left[\int_{l_o}\left\{\mathbf{H}_1^{\mathrm{T}} A_\rho \ddot{\mathbf{u}}^e + \mathbf{H}_2^{\mathrm{T}}\left[\mathbf{I}_\rho^e \ddot{\mathbf{w}}^e + \widetilde{\dot{\mathbf{w}}^e}\mathbf{I}_\rho^e \dot{\mathbf{w}}^e\right]\right\}\mathrm{d}l\right], \tag{60}$$

with (see Eq. (37))

$$\mathbf{I}_\rho^e = \mathbf{R}_r{}^{\mathrm{T}}\,\mathbf{I}_\rho\,\mathbf{R}_r = \overline{\mathbf{R}}\,\mathbf{J}_\rho\,\overline{\mathbf{R}}^{\mathrm{T}}. \tag{61}$$

$\overline{\mathbf{R}}$ is the rotation matrix associated with the local rotation of the section (see Fig. 4).
As shown in the above equation, the inertia force vector depends on $\mathbf{d}_g, \dot{\mathbf{d}}_g$ and $\ddot{\mathbf{d}}_g$. Hence, linearization of this force vector is evaluated as follows

$$\Delta\mathbf{f}_{\mathrm{k}} = \mathbf{M}\Delta\ddot{\mathbf{d}}_g + \mathbf{C}_{\mathrm{k}}\Delta\dot{\mathbf{d}}_g + \mathbf{K}_{\mathrm{k}}\Delta\mathbf{d}_g\,. \tag{62}$$

Some authors proposed to keep only the mass matrix $\mathbf{M}$, and to eliminate the gyroscopic $\mathbf{C}_{\mathrm{k}}$ and centrifugal $\mathbf{K}_{\mathrm{k}}$ dynamic matrices [9, 19]. However, in [27], extensive numerical studies have shown that it is better to keep also the gyroscopic matrix in order to enhance the computational efficiency. The same approach is used here. The centrifugal matrix, whose derivation is complicated and would give a large mathematical expression, is neglected. Therefore, the iterative scheme of the present formulation is implemented with the following approximative linearization

$$\Delta\mathbf{f}_{\mathrm{k}} \approx \mathbf{M}\Delta\ddot{\mathbf{d}}_g + \mathbf{C}_{\mathrm{k}}\Delta\dot{\mathbf{d}}_g\,. \tag{63}$$

The explicit expressions of the mass matrix $\mathbf{M}$ and of the gyroscopic matrix $\mathbf{C}_{\mathrm{k}}$ are given by

$$\mathbf{M} = \mathbf{E}\left\{\int_{l_o}\left(\mathbf{H}_1^{\mathrm{T}} A_\rho\,\mathbf{H}_1 + \mathbf{H}_2^{\mathrm{T}}\mathbf{I}_\rho^e\,\mathbf{H}_2\right)\mathrm{d}l\right\}\mathbf{E}^{\mathrm{T}} = \mathbf{E}\,\mathbf{M}^e\,\mathbf{E}^{\mathrm{T}}, \tag{64}$$

$$\begin{aligned}\mathbf{C}_{\mathrm{k}} =& \mathbf{E}\left\{\int_{l_o}\mathbf{H}_1^{\mathrm{T}} A_\rho\,(\mathbf{C}_1+\mathbf{C}_3)\,\mathrm{d}l + \int_{l_o}\mathbf{H}_2^{\mathrm{T}}\mathbf{I}_\rho^e\,(\mathbf{C}_2+\mathbf{C}_4)\,\mathrm{d}l\right.\\ &\left.+\int_{l_o}\mathbf{H}_2^{\mathrm{T}}\left(\widetilde{\dot{\mathbf{w}}^e}\mathbf{I}_\rho^e - \widetilde{\mathbf{I}_\rho^e\dot{\mathbf{w}}^e}\right)\mathbf{H}_2\mathrm{d}l\right\}\mathbf{E}^{\mathrm{T}} = \mathbf{E}\,\mathbf{C}_{\mathrm{k}}^e\,\mathbf{E}^{\mathrm{T}},\end{aligned} \tag{65}$$

with $\mathbf{C}_3$ and $\mathbf{C}_4$ given in Appendix B.

6.4 Numerical integration

The internal force vector $\mathbf{f}_{\mathrm{g}}$ and the tangent stiffness matrix $\mathbf{K}_{\mathrm{g}}$ are exactly evaluated without numerical integrations.

Concerning the dynamic terms, i.e. the inertia force vector $\mathbf{f}_{\mathrm{k}}$, the mass matrix $\mathbf{M}$ and the gyroscopic matrix $\mathbf{C}_{\mathrm{k}}$, two approaches have been implemented. The first one, referred to "cubic corotational approach", is the one presented in this section. Three Gauss points are used to integrate Eqs. (60), (64) and (65). The second approach, referred to "linear corotational approach", is obtained by assuming linear interpolations for all local quantities. This mean that the cubic interpolations N_5 and N_6 are replaced with N_1 and N_2 in Eq. (30), and that the local transverse

displacements $\overline{u}_2$ and $\overline{u}_3$ are zero (see Eq. (30)). For this linear approach, two Gauss points are used to calculate the inertia force vector and the tangent dynamic matrix. It can be observed that linear local interpolations imply $\mathbf{u}_l = \mathbf{0}_{3\times 1}$, which simplifies significantly the computations.

It should be noted that, in these two corotational approaches, all the quantities at the Gauss point are directly calculated from the nodal ones. Therefore, no extra storage is needed.

7 Numerical examples

The purpose of this section is to assess both the cubic and the linear corotational formulations. The first one employs cubic interpolation for all terms whereas the second uses cubic interpolation for the internal force vector and the corresponding stiffness matrix, the inertia terms being evaluated considering linear interpolation. The predictions of these formulations are compared against the total Lagrangian formulation proposed by Simo and Vu-Quoc [35, 36, 37]. In this formulation which employs spatial spin variables, the internal force vector and the tangent stiffness matrix are numerically integrated using one Gauss point whereas the inertia force vector and the dynamic tangent matrix are numerically integrated using two Gauss points. All the three formulations are implemented using Matlab. The same levels of optimisation in forming the element matrices and force vectors are carefully checked.

Several numerical applications are considered. For each application, the solutions given by the three dynamic formulations are compared against a reference solution. The latter is obtained by increasing the number of elements until the three dynamic formulations converge towards the same results.

The first numerical example has been proposed by Simo and Vu-Quoc [37]. This problem is very popular and has been considered by many authors as a test for nonlinear dynamic formulations involving large rotations. In this example, the reference solution is in a good agreement with the results found in the literature. For the second example, additional analyses with Abaqus are performed in order to assess the quality of the reference solutions. Two different beam elements are used. The first one is B31, which is based on the classical Timoshenko beam theory. The second one is B33, which is based on the classical Euler-Bernoulli beam theory. With refined meshes and refined time step sizes, these two elements converged towards the selected reference solutions. It can also be concluded that the shear effects are very small and can be neglected.

In their work, Simo and Vu-Quoc [37] employed the Newmark trapezoidal rule. When applied to nonlinear dynamics, this scheme can be unstable [10, 24, 41]. To avoid this problem, the HHT α method [13] with $\alpha = -0.05$ is employed in this work. This value of α, which is typically adopted in nonlinear dynamic analyses [9, 12, 24] and also used as default in Abaqus, gives a small numerical damping and limits the influence of high frequencies. However, a numerical damping gives also a dissipation of the total energy, which can affect long time analyses.

During the time period under consideration, the time step size remains constant. Except for the first example, where the time step size is taken as in the literature [20, 23, 24, 37, 44], the time step size is carefully selected. For that, the same example is run using $0.5\,\Delta t$. The time step is accepted if both runs provide the same results.

At the beginning of each time step, a predictor is used to initiate the iterative procedure. Several predictors are available in the literature and a comparative study of the performances of these predictors can be found in [27]. As shown in [27], the quality of the predictor has a significant influence on the convergence of the iterative procedure. In the present work, the predictor proposed by Crisfield [13] for the particular case of linear inertia force vector and further developed in the general case by the authors [27], is adopted. The idea of this predictor is to use the tangent operator at the time instant t_n to predict the values at the time instant t_{n+1}. This predictor is the most effective among the four ones compared in [27].

Damping is not considered and the following convergence criterion is adopted: the norm of the residual vector must be less than the prescribed tolerance $\varepsilon_f = 10^{-5}$.

7.1 Example 1: Right-angle cantilever beam

This classic example, introduced by Simo and Vu-Quoc [37], has often been used in order to validate various nonlinear dynamic formulations [19, 20, 24, 28]. A right-angle cantilever, depicted in Fig. 5, is subjected to an out-of-plane concentrated load applied at the elbow. Each member of the cantilever has a length $L = 10$. The material properties are $GA = EA = 10^6$, $GJ = EI = 10^3$. The mass per unit length of the beam and the inertia dyadic of the cross section in the initial configuration are $A_\rho = 1$ and $\mathbf{J}_\rho = \mathrm{diag}(20, 10, 10)$, respectively.
The load (see Fig. 6) acts only during $0 \leq t(s) \leq 2$ and thereafter the cantilever undergoes large-scale free vibrations. The applied force increases linearly until the value of 50 is reached at one second and decreases from there to zero within one further second. The resulting amplitude of vibration is of the same order of magnitude as the structure's dimensions. The reference solution has been obtained with a total of 20 beam elements (10 elements per member) whereas the predictions of the three aforementioned formulations have derived using only 4 elements (2 elements per member).
The time evolution of the out-of-plane displacement of node A is depicted in Fig. 7. The

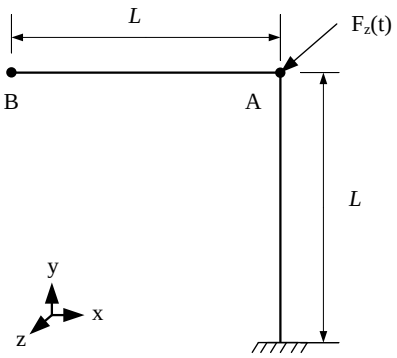

Figure 5: Right-angle cantilever beam : geometrical data.

computations are performed with $\Delta t = 0.25$ s. It can be noted that with only 4 beam elements, the cubic corotational approach gives almost the same results as the reference solution over the whole time domain. The results obtained with the linear corotational approach are very close to

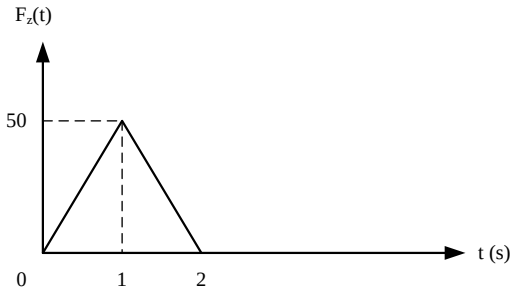

Figure 6: Right-angle cantilever beam - Loading history.

the reference solution with minor differences. However, the results obtained with the formulation of Simo and Vu-Quoc are far from the reference solution.

The time evolution of the out-of-plane displacement of node B, calculated with a total of 8

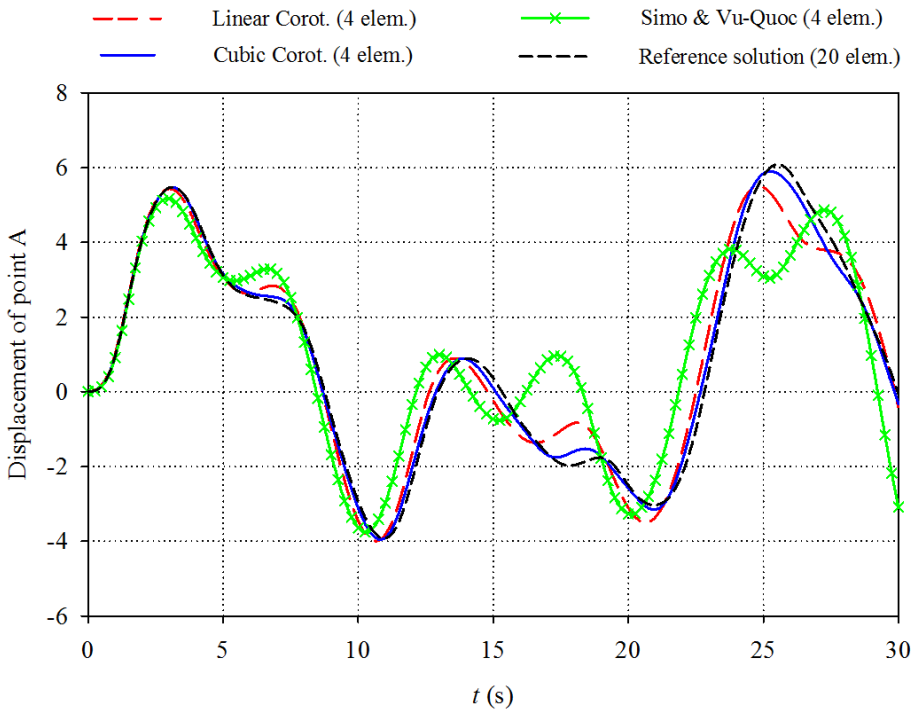

Figure 7: Right-angle cantilever beam - Time evolution of the out-of-plane displacement of point A.

beam elements (4 elements per member), is depicted in Fig. 8. It can be noted that the differences between the formulation of Simo and Vu-Quoc and the reference solution become smaller, but also that the cubic corotational formulation gives very accurate results.

In the current example, the energy blow-up can happen at approximately $t = 45$ s. This numerical instability has been reported by Jelenić and Crisfield [23, 24] and by Zupan et al. [44]. Therefore, to assess the stability of the HHT α method when combined with the new cubic formulation, this example is run for a time period of 150 s using a total of 20 beam elements

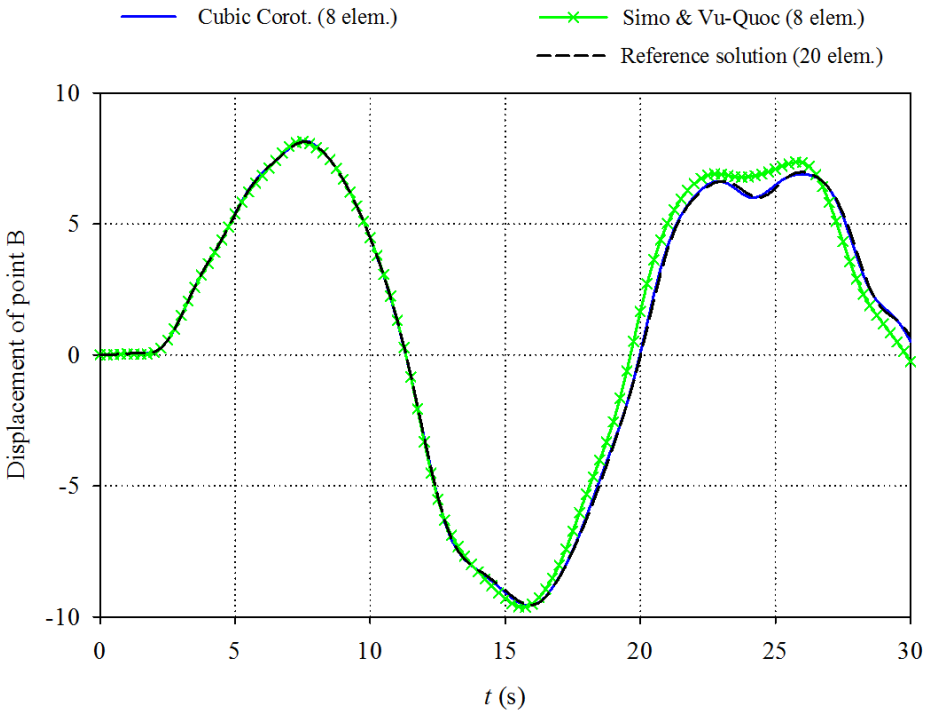

Figure 8: Right-angle cantilever beam - Time evolution of the out-of-plane displacement of point B.

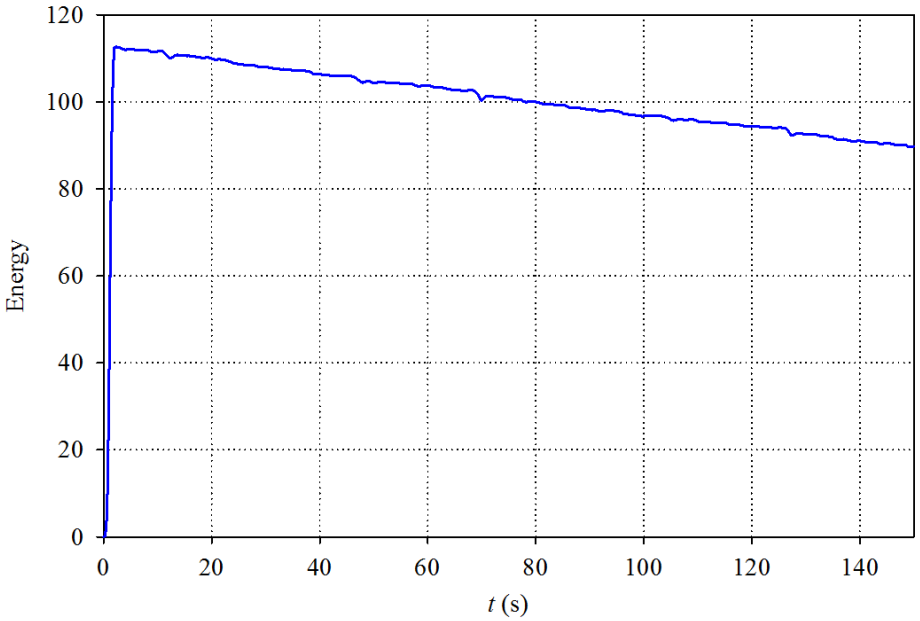

Figure 9: Right-angle cantilever beam - Time evolution of the total energy.

and a time step $\Delta t = 0.25$ s. The time evolution of the total energy is depicted in Fig. 9. The result indicates that the new formulation is stable during the time period under consideration. The dissipation of energy between $t = 2$ s and $t = 30$ s is about 3%.

The CPU time and the total number of iterations required for each formulation are presented

Table 1: Right-angle cantilever beam - CPU time (Total number of iterations).

Number of beam elements	Linear corot.	Cubic corot.	Simo & Vu-Quoc
4	3.66 (633)	5.31 (637)	4.59 (521)
20	19.84 (636)	25.61 (612)	22.90 (517)

in Tab. 1. With the same number of elements, the linear corotational approach is the fastest approach and the cubic corotational approach is the slowest one.

7.2 Example 2: Cantilever beam

The second example is a cantilever beam of length $L = 10$ m with uniform cross-section (see Fig. 10). The beam is clamped at one end and subjected to a sinusoidal out-of-plane force $F_z(t)$ and a bending moment $M_z(t)$ at the free end (see Fig. 11). The circular frequency of the force w is 50 rad/s. The bending moment increases linearly until the value of 3 is reached at 0.3 second and decreases from there to zero within a further 0.3 second. The cross-section width and depth are $e = 0.25$ m and $a = 0.3$ m, respectively. The elastic modulus of the beam E is 210 GPa and the Poisson's ratio ν is 0.3. The mass per unit volume is $\rho = 7850$ kg/m^3.
The time step size is chosen as $\Delta t = 5 \cdot 10^{-4}$ s.

The reference solution has been obtained with a total of 20 beam elements whereas only

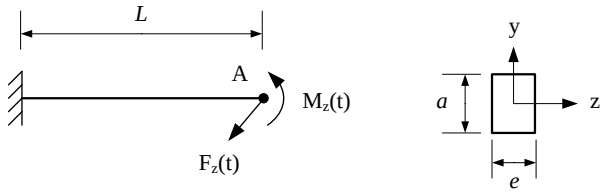

Figure 10: Cantilever beam : geometrical data.

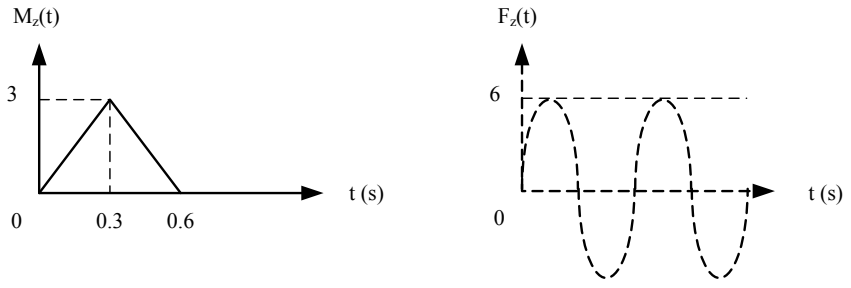

Figure 11: Cantilever beam - Loading history.

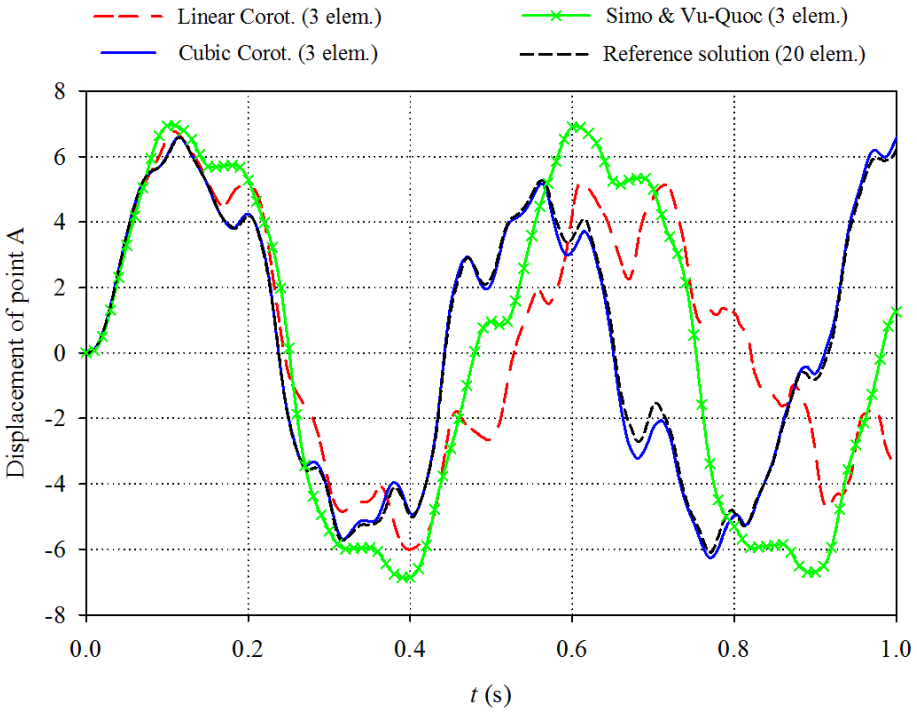

Figure 12: Cantilever beam - Time evolution of the out-of-plane displacement of point A.

Table 2: Cantilever beam - CPU time (Total number of iterations).

Number of beam elements	Linear corot.	Cubic corot.	Simo & Vu-Quoc
3	24.97 (5844)	34.22 (5829)	27.45 (4339)
20	164.86 (5346)	227.01 (5486)	220.94 (5394)

3 beam elements are used for the computations with the three formulations. The out-of-plane displacement of the free end A is depicted in Fig. 12.
It can be noted that the results obtained with the cubic corotational approach are very close to the reference solution. However, large discrepancies between the results obtained with the two other formulations and the reference solution can be observed. As for the first example, with the same number of elements, the linear corotational approach is the fastest formulation and the cubic corotational approach is the slowest one (see Tab. 2).

8 Conclusion

A new consistent 3D corotational beam element for nonlinear dynamics of flexible structures was presented. The novelty of the formulation is that the corotational framework (i.e. the decomposition into rigid body motion and pure deformation) was adopted to formulate not only the internal force vector and the tangent stiffness matrix, but also the inertia force vector and the tangent dynamic matrix. As consequence, the cubic interpolation functions were used to derive both the inertia and internal local terms. The inertia force vector and the tangent dynamic matrix were analytically formulated by introducing an approximation regarding the local rotations. To enhance the efficiency of the iterative procedure, an approximative tangent dynamic matrix was adopted.

Several numerical examples were considered to compare the new formulation with two other approaches. The first approach, called as "linear corotational approach", is derived from the new formulation by replacing cubic interpolations with linear ones. The second approach is the classic total Lagrangian proposed by Simo and Vu-Quoc [35, 36, 37]. Based on these examples, the following conclusions can be drawn:

- All formulations give the same results with fine meshes.
- With coarse meshes, Simo and Vu-Quoc's formulation and the linear corotational one give less accurate results compared to the cubic corotational approach which provides very accurate results. This demonstrated the importance of an accurate description of the deformations in the dynamic terms, which is not possible with linear interpolations (Simo and Vu-Quoc's formulation adopted linear interpolations for all the global variables).
- The linear corotational approach is faster than the cubic one. This was expected since several inertia terms disappear when local linear interpolations are adopted. Moreover, in the linear corotational approach, the inertia force vector and the tangent dynamic matrix are integrated using two Gauss points, whereas the dynamic terms of the cubic corotational one are integrated using three Gauss points.
- The cubic corotational approach is slightly slower (about 12%) and sometimes even faster than Simo and Vu-Quoc's one.

One can conclude that the new dynamic corotational formulation based on the local cubic interpolations is more efficient than the classic one proposed by Simo and Vu-Quoc. With the same number of elements, about the same computational time is required (this can differ a little from one example to another). However, with the present formulation, accurate results can be obtained with a smaller number of elements.

A Expressions of $\dot{\mathbf{H}}_1$ and $\dot{\mathbf{H}}_2$

The variation of Eq. (49) reads

$$\delta\mathbf{H}_1 = \mathbf{P}_1\,\delta\mathbf{P} - \widetilde{\delta\mathbf{u}_l}\,\mathbf{G}^{\mathrm{T}} - \widetilde{\mathbf{u}_l}\,\delta\mathbf{G}^{\mathrm{T}}, \tag{66}$$

where $\mathbf{u}_l$ are the local transverse displacements assumed to be small. Therefore, the last term in Eq. (66) is neglected.
By using the expressions of the matrices $\mathbf{P}_1$ and $\mathbf{P}$, and the variation of Eq. (9), it is straightforward to obtain

$$\delta\mathbf{H}_1 = \frac{N_7}{l_n^2}\,\mathbf{A}_1\,\mathbf{r}\,\delta\mathbf{d}_g - \widetilde{\delta\mathbf{u}_l}\,\mathbf{G}^{\mathrm{T}}, \tag{67}$$

with $N_7 = (N_3 + N_4)$, $\mathbf{r} = \begin{bmatrix} -\mathbf{r}_1^{\mathrm{T}} & \mathbf{0}_{[1\times3]} & \mathbf{r}_1^{\mathrm{T}} & \mathbf{0}_{[1\times3]} \end{bmatrix}$ and

$$\mathbf{A}_1 = \begin{bmatrix} 0 & 0 & 0 & 0 & 0 & 0 & 0 & 0 & 0 & 0 & 0 & 0 \\ 0 & -1 & 0 & 0 & 0 & 0 & 0 & 1 & 0 & 0 & 0 & 0 \\ 0 & 0 & -1 & 0 & 0 & 0 & 0 & 0 & 1 & 0 & 0 & 0 \end{bmatrix}.$$

Finally, one has

$$\dot{\mathbf{H}}_1 = \frac{N_7}{l_n^2}\mathbf{A}_1\,\mathbf{r}\,\dot{\mathbf{d}}_g - \widetilde{\dot{\mathbf{u}}}_l\,\mathbf{G}^{\mathrm{T}}. \tag{68}$$

By taking the variation of Eq.(56), and using the expressions of $\mathbf{P}_2$, $\mathbf{P}$ and $\mathbf{G}$, one obtains

$$\delta\mathbf{H}_2 = \frac{N_8}{l_n^2}\mathbf{A}_2\,\mathbf{r}\,\delta\mathbf{d}_g. \tag{69}$$

with $N_8 = N_5 + N_6 - 1$ and

$$\mathbf{A}_2 = \begin{bmatrix} 0 & 0 & 0 & 0 & 0 & 0 & 0 & 0 & 0 & 0 & 0 & 0 \\ 0 & 0 & 1 & 0 & 0 & 0 & 0 & 0 & -1 & 0 & 0 & 0 \\ 0 & -1 & 0 & 0 & 0 & 0 & 0 & 1 & 0 & 0 & 0 & 0 \end{bmatrix}.$$

Therefore, $\dot{\mathbf{H}}_2$ is computed as

$$\dot{\mathbf{H}}_2 = \frac{N_8}{l_n^2}\mathbf{A}_2\,\mathbf{r}\,\dot{\mathbf{d}}_g. \tag{70}$$

B Expressions of $\mathbf{C}_3$ and $\mathbf{C}_4$

$\mathbf{C}_3$ and $\mathbf{C}_4$ are calculated from the variations of $\mathbf{C}_1$ and $\mathbf{C}_2$ with respect to $\dot{\mathbf{d}}_g$

$$\mathbf{C}_3\,\mathbf{E}^{\mathrm{T}}\Delta\dot{\mathbf{d}}_g = \left(\frac{\partial\mathbf{C}_1}{\partial\dot{\mathbf{d}}_g}\Delta\dot{\mathbf{d}}_g\right)\mathbf{E}^{\mathrm{T}}\dot{\mathbf{d}}_g, \tag{71}$$

$$\mathbf{C}_4\,\mathbf{E}^{\mathrm{T}}\Delta\dot{\mathbf{d}}_g = \left(\frac{\partial\mathbf{C}_2}{\partial\dot{\mathbf{d}}_g}\Delta\dot{\mathbf{d}}_g\right)\mathbf{E}^{\mathrm{T}}\dot{\mathbf{d}}_g, \tag{72}$$

After some long but straightforward manipulations, the expressions of $\mathbf{C}_3$ and $\mathbf{C}_4$ are obtained as

$$\mathbf{C}_3 = -\widetilde{\mathbf{h}}_1\,\mathbf{G}^{\mathrm{T}} + \left(\frac{N_7}{l_n^2}\mathbf{A}_1\,\dot{\mathbf{d}}_g^e\,\mathbf{r}^e + \widetilde{\dot{\mathbf{w}}}_r^e\mathbf{P}_1\,\mathbf{P}\right) + \mathbf{H}_1\,\mathbf{F}_1\,\mathbf{G}^{\mathrm{T}}, \tag{73}$$

$$\mathbf{C}_4 = -\widetilde{\mathbf{h}}_2\,\mathbf{G}^{\mathrm{T}} + \frac{N_8}{l_n^2}\mathbf{A}_2\,\dot{\mathbf{d}}_g^e\,\mathbf{r}^e + \mathbf{H}_2\,\mathbf{F}_1\,\mathbf{G}^{\mathrm{T}}, \tag{74}$$

with

$$\mathbf{h}_i = \mathbf{H}_i\dot{\mathbf{d}}_g^e, \quad \mathbf{F}_1 = [\widetilde{\dot{\mathbf{u}}}_1^{e\,\mathrm{T}}\,\widetilde{\dot{\mathbf{w}}}_1^{e\,\mathrm{T}}\,\widetilde{\dot{\mathbf{u}}}_2^{e\,\mathrm{T}}\,\widetilde{\dot{\mathbf{w}}}_2^{e\,\mathrm{T}}]^{\mathrm{T}}, \tag{75}$$
$$\mathbf{r}^e = \mathbf{r}\,\mathbf{E} = \left[-[1\,0\,0]\;\;\mathbf{0}_{[1\times3]}\;\;[1\,0\,0]\;\;\mathbf{0}_{[1\times3]}\right].$$

REFERENCES

[1] R. Alsafadie, M. Hjiaj, J.-M. Battini, Corotational mixed finite element formulation for thin-walled beams with generic cross-section, *Comput. Methods Appl. Mech. Engrg.*, **199**, 3197-3212, 2010.

[2] R. Alsafadie, J.-M. Battini, M. Hjiaj, H. Somja, A comparative study of displacement and mixed-based corotational finite element formulations for elasto-plastic three-dimensional beam analysis, *Engerg. Computs.*, **28**, 7, 939-982, 2011.

[3] J. Argyris, An excursion into large rotations, *Comput. Methods Appl. Mech. Engrg.*, **32**, 85-155, 1982.

[4] J.-M. Battini, C. Pacoste, Co-rotational beam elements with warping effects in instability problems, *Comput. Methods Appl. Mech. Engrg.*, **191**, 1755-1789, 2002.

[5] J.-M. Battini, A modified corotational framework for triangular shell elements, *Comput. Methods Appl. Mech. Engrg.*, **196**, 1905-1914, 2007.

[6] J.-M. Battini, Large rotations and nodal moments in corotational elements, *CMES*, **33**, 1, 1-15, 2008.

[7] K. Behdinan, M.C Stylianou, B. Tabarrok, Co-rotational dynamic analysis of flexible beams, *Comput. Methods Appl. Mech. Engrg.*, **154**, 151-161, 1998.

[8] P. Betsch, P. Steinmann, Constrained dynamics of geometrically exact beams, *Comput. Mech.*, **31**, 49-59, 2003.

[9] A. Cardona, M. Geradin, A beam finite element non-linear theory with finite rotations, *Int. J. Num. Methods. Engrg.*, **26**, 2403-2438, 1988.

[10] M.A. Crisfield, J. Shi, An energy conserving co-rotational procedure for non-linear dynamics with finite elements, *Nonlinear Dynamics*, **9**, 37-52, 1996.

[11] M.A. Crisfield, G.F. Moita, A unified co-rotational framework for solids shells and beams, *Int. J. Solids Struct.*, **33**, 29692992, 1996.

[12] M.A. Crisfield, U. Galvanetto, G. Jelenić, Dynamics of 3-D co-rotational beams, *Comput. Mech.*, **20**, 507-519, 1997.

[13] M.A. Crisfield, *Non-Linear Finite Element Analysis of Solids and Structures, Volume 2: Advanced Topics*, Wiley, Chischester, 1997.

[14] H.A. Elkaranshawy and M.A. Dokainish, Corotational finite element analysis of planar flexible multibody systems, *Comput. Struct.*, **54**, No.5, 881-890, 1995.

[15] U. Galvanetto, M.A. Crisfield, An energy conserving co-rotational procedure for dynamics of planar beam structures, *Int. J. Num. Methods. Engrg.*, **39**, 2265-2282, 1996.

[16] M. Geradin, A. Cardona, Kinematics and dynamics of rigid and flexible mechanisms using finite elements and quaternion algebra, *Comput. Mech.*, **4**, 115-135, 1989.

[17] M. Geradin, A. Cardona, *Flexible multibody dynamics : A finite element approach*, 120-127. Wiley, Chischester, 2001.

[18] K.M. Hsiao, R.T. Yang, A co-rotational formulation for nonlinear dynamic analysis of curved Euler beam, *Comput. Struct.*, **54**, No.6, 1091-1097, 1995.

[19] K.M. Hsiao, J.Y. Lin, W.Y. Lin, A consistent co-rotational finite element formulation for geometrically nonlinear dynamics analysis of 3-D beams, *Comput. Methods Appl. Mech. Engrg.*, **169**, 1-18, 1999.

[20] A. Ibrahimbegović, M.A. Mikdad, Finite rotations in dynamics of beams and implicit time-stepping schemes, *Int. J. Num. Methods. Engrg.*, **41**, 781-814, 1998.

[21] M. Iura, S.N. Atluri, Dynamic analysis of finitely stretched and rotated three-dimensional space-curved beams, *Comput. Struct.*, **29**, 875-889, 1988.

[22] M. Iura, S.N. Atluri, Dynamic analysis of planar flexible beams with finite rotations by using inertial and rotating frames, *Comput. Struct.*, **55**, No.3, 453-462, 1995.

[23] G. Jelenić, M.A. Crisfield, Interpolation of rotational variables in nonlinear dynamics of 3D beams, *Int. J. Num. Methods. Engrg.*, **43**, 1193-1222, 1998.

[24] G. Jelenić, M.A. Crisfield, Geometrically exact 3D beam theory: implementation of a strain-invariant element for stactics and dynamics, *Comput. Methods Appl. Mech. Engrg.*, **171**, 141-171, 1999.

[25] S. Krenk, *Non-Linear Modeling And Analysis Of Solids And Structures*, 47-75, Cambridge University Press, New York, 2009.

[26] T.-N. Le, J.-M. Battini, M. Hjiaj, Efficient formulation for dynamics of corotational 2D beams, *Comput. Mech.*, **48**, No.2, 153-161, 2011.

[27] T.-N. Le, J.-M. Battini, M. Hjiaj, Dynamics of 3D beam elements in a corotational context: A comparative study of established and new formulations, *Finite Elem. Anal. Des.*, **61**, 97-111, 2012.

[28] J. Mäkinen, Total Lagrangian Reissner's geometrically exact beam element without singularities, *Int. J. Num. Methods. Engrg.*, **70**, 1009-1048, 2007.

[29] N. Masuda, T. Nishiwaki, M. Minaaawa, Nonlinear dynamic analysis of frame structures, *Comput. Struct.*, **27**, No.1, 103-110, 1987.

[30] B. Nour-Omid, C.C. Rankin, Finite rotation analysis and consistent linearization using projectors, *Comput. Methods Appl. Mech. Engrg.*, **93**, 353-384, 1991.

[31] C. Oran, A. Kassimali, Large deformations of framed structures under static and dynamic loads, *Comput. Struct.*, **6**, 539-547, 1976.

[32] C. Pacoste, A. Eriksson, Beam elements in instability problems, *Comput. Methods Appl. Mech. Engrg.*, **144**, 163-197, 1997.

[33] C. Pacoste, Co-rotational flat facet triangular elements for shell instability analysis, *Comput. Methods Appl. Mech. Engrg.*, **156**, 75110, 1998.

[34] J.N. Reddy, On locking-free shear deformable beam finite elements, *Comput. Methods Appl. Mech. Engrg.*, **149**, 113-132, 1997.

[35] J.C. Simo, A finite strain beam formulation. The three-dimensional dynamic problem. Part I, *Comput. Methods Appl. Mech. Engrg.*, **49**, 55-70, 1985.

[36] J.C. Simo, L. Vu-Quoc, A three-dimensional finite-strain rod model. Part II: computational aspects, *Comput. Methods Appl. Mech. Engrg.*, **58**, 79-116, 1986.

[37] J.C. Simo, L. Vu-Quoc, On the dynamics in space of rods undergoing large motions - A geometrically exact approach, *Comput. Methods Appl. Mech. Engrg.*, **66**, 125-161, 1988.

[38] Q. Xue, J.L Meek, Dynamic response and instability of frame structures, *Comput. Methods Appl. Mech. Engrg.*, **190**, 5233-5242, 2001.

[39] A. Ibrahimbegović, F. Frey, I. Kožar, Computational aspects of vector-like parameterization of three-dimensional finite rotations, *Int. J. Num. Methods. Engrg.*, **38**, 3653-3673, 1995.

[40] A. Ibrahimbegović, On the choice of finite rotation parameters, *Comput. Methods Appl. Mech. Engrg.*, **149**, 49-71, 1997.

[41] H. Weiss , Dynamics of geometrically nonlinear rods: II. Numerical methods and computational examples, *Nonlinear Dynamics*, **30**, 383-415, 2002.

[42] E.V. Lens, A. Cardona, A nonlinear beam element formulation in the framework of an energy preserving time integration scheme for constrained multibody systems dynamics, *Comput. Struct.* , **86**, 47-63, 2008.

[43] E. Zupan, M. Saje, D. Zupan, Quaternion-based dynamics of geometrically nonlinear spatial beams using the RungeKutta method, *Finite Elem. Anal. Des.*, **54**, 48-60, 2012.

[44] E. Zupan, M. Saje, D. Zupan, Dynamics of spatial beams in quaternion description based on the Newmark integration scheme, *Comput. Mech.*, **51**, 47-64, 2013.